

# Tidal Disruption of Satellite Galaxies in a Semi-Analytic Model of Galaxy Formation

Bruno M. B. Henriques<sup>1,2\*</sup>, Peter A. Thomas<sup>2</sup>

<sup>1</sup>*Institute of Cosmology and Gravitation, University of Portsmouth, Portsmouth PO1 3FX, United Kingdom*

<sup>2</sup>*Astronomy Centre, University of Sussex, Falmer, Brighton BN1 9QH, United Kingdom*

Submitted to MNRAS

## ABSTRACT

We introduce a new physical recipe into the De Lucia and Blaizot version of the Munich semi-analytic model built upon the Millennium dark matter simulation: the tidal stripping of stellar material from satellite galaxies during mergers.

To test the significance of the new physical process we apply a Monte Carlo Markov Chain parameter estimation technique constraining the model with the  $K$ -band luminosity function,  $B - V$  colours and the black hole-bulge mass relation. The differences in parameter correlations, and in the allowed regions in likelihood space, reveal the impact of the new physics on the basic ingredients of the model, such as the star-formation laws, feedback recipes and the black hole growth model.

With satellite disruption in place, we get a model likelihood four times higher than in the original model, indicating that the new process seems to be favoured by observations. This is achieved mainly due to a reduction in black hole growth that produces a better agreement between the properties of central black holes and host galaxies. Compared to the best-fit model without disruption, the new model removes the excess of dwarf galaxies in the original recipe with a more modest supernova heating.

The new model is now consistent with the three observational data sets used to constrain it, while significantly improving the agreement with observations for the distribution of metals in stars. Moreover, the model now has predictions for the intra-cluster light, a very significant component of large groups and clusters, that agree with observational estimates.

**Key words:** methods: numerical – methods: statistical – galaxies: formation – galaxies: evolution

## 1 INTRODUCTION

In recent years, semi-analytic (SA) models have experienced a significant degree of success, achieving a considerable agreement with a large set of observational properties. These range from the luminosity to the stellar mass functions, Tully-Fisher relations, clustering, galaxy colours, etc (Bower et al. 2006; Croton et al. 2006).

Some fundamental changes determined the improvements achieved. First of all, these recipes were implemented on top of a direct dark matter simulation, which just recently have been able to simulate cosmological volumes with a large enough resolution to follow haloes containing dwarf galaxies (the Millennium run, Springel et al. 2005). Secondly, some key physical recipes were introduced:

the energy feedback from supernovae explosions, which for small enough galaxies and strong enough explosions can drive the gas out of the galaxy (Benson et al. 2003; De Lucia et al. 2004); and the feedback from central black holes, which determines the properties of massive galaxies (Granato et al. 2004; Bower et al. 2006; Cattaneo et al. 2006; Croton et al. 2006; Menci et al. 2006; Monaco et al. 2007; Somerville et al. 2008).

The level of agreement achieved opens up a number of possibilities. This agreement can now be quantified against different observational data sets using robust statistical tests (Kampakoglou et al. 2008; Henriques et al. 2009, hereafter Paper 1). This means that the allowed likelihood regions in parameter space can be obtained and confidence limits for the preferred parameter values can be built. Moreover, with the physics that determine the global properties of galaxies reasonably well understood, modellers can now focus on ad-

\* E-mail: Bruno.Henriques@port.ac.uk

ditional ingredients that determine the fine tuning of galaxies properties.

Amongst these detailed studies we can find the stripping of gas from satellite galaxies (Font et al. 2008); the impact of the assumed dust model on the overall galaxy properties (De Lucia & Blaizot 2007) and on the galaxy clustering over redshift (Guo & White 2009); the impact of quasar mode feedback on the luminosity-temperature (L-T) relation in clusters (Bower et al. 2008); and the effects of a dynamical treatment of galactic winds on host galaxies (Bertone et al. 2007).

Another physical process that is becoming more relevant in theoretical models is the disruption of stellar material from merging satellites due to tidal stripping, with studies being performed using both the semi-analytic (Bullock et al. 2001; Taylor & Babul 2001; Benson et al. 2002; Monaco et al. 2007; Henriques et al. 2008; Somerville et al. 2008; Seek Kim et al. 2009) and the Halo Occupation Distribution (HOD) approach (Yang et al. 2009; Wetzel & White 2009).

Evidence for the importance of this process in galaxy formation comes from various fields. The existence of a diffuse population of intra-cluster stars was first proposed by Zwicky (1951) and has since been detected unambiguously (Durrell et al. 2002; Gal-Yam et al. 2003; Neill et al. 2005; Krick et al. 2006). The light associated with intra-cluster stars, or diffuse intra-cluster light (ICL), can contribute between 10 and 40 per cent of the optical emission of rich galaxy groups and clusters (Bernstein et al. 1995; Gonzalez et al. 2000; Feldmeier et al. 2002; Feldmeier et al. 2004; Gonzalez et al. 2005; Zibetti et al. 2005).

Rather than having formed in the intra-cluster medium, gas-dynamical simulations generally agree that the bulk of the ICL is emitted by stars that have been continually stripped from member galaxies throughout the lifetime of a cluster, or have been ejected into intergalactic space by merging galaxy groups (Moore et al. 1996; Napolitano et al. 2003; Murante et al. 2004; Willman et al. 2004; Sommer-Larsen et al. 2005; Monaco et al. 2006; Murante et al. 2007; Rudick et al. 2009).

Observationally, low surface brightness features have been identified in the Coma and Centaurus clusters (Gregg & West 1998; Trentham & Mobasher 1998; Feldmeier et al. 2002), indicating the presence of dynamically-young tidal structures produced by the disruption of infalling galaxies. Moreover, Faltenbacher & Mathews (2005) show that the projected number density profile of dwarf galaxies in NGC 5044 can only be explained by assuming that a significant amount of mass in satellite galaxies is tidally disrupted.

If, as the evidence suggests, intra-cluster stars are the remnants of material stripped from merging satellites, the build up of this component can be directly followed by a semi-analytic model with a self consistent implementation of tidal disruption (Bullock et al. 2001; Taylor & Babul 2001; Benson et al. 2002; Monaco et al. 2006; Somerville et al. 2008). Also, the disruption of material from satellite galaxies might play a crucial role in solving a common problem to most semi-analytic models: the excess of dwarf galaxies (Henriques et al. 2008; Weinmann et al. 2006).

Despite the fact that a number of authors have introduced satellite disruption in theoretical models of galaxy

formation, the complexity of these models makes it difficult to fully understand the impact of different physics on the global galaxy properties. Also, the number of free parameters makes it some times impossible to take full advantage of the new physics introduced, when a manual tuning fails to reach the best possible fit.

In this paper we make use of the Monte Carlo Markov Chain (MCMC) statistical techniques introduced in Henriques et al. (2009) to test the impact of satellite disruption in semi-analytic models of galaxy formation. With the introduction of a new physical recipe, both the normalisation and shapes of the acceptable likelihood regions contain useful information that can be used to discriminate between models. We will show that the new model is favored by the data, that it provides a better fit to the metallicity of galaxies than our previous model, and that it predicts ICL fractions that agree with observations. We note that similar MCMC techniques were proposed independently by Kampakoglou et al. (2008) to test the impact of different star formation modes in their specific semi-analytic recipe.

This paper is organized as follows. In Section 2, we describe the original semi-analytic model used in our study and the new implementation of satellite disruption. Section 3 presents results from a model with disruption using the same parameters as in the original recipe to directly test the differences between the two. In Section 4 we briefly describe the MCMC techniques introduced in Paper 1. In Section 5 we present the best fit model with satellite disruption and compared its likelihood maximum, acceptable likelihood regions and galaxy predictions with the previous model. Finally in Section 6 we summarize our conclusions.

## 2 THE MODEL

To perform the work described in this paper we used the Munich SA recipe as described in Croton et al. (2006) and De Lucia & Blaizot (2007, hereafter DLB07). It is built on top of a direct numerical simulations of the dark matter structure in a cosmological volume, the Millennium Simulation (Springel et al. 2005). This simulation traces the evolution of dark matter haloes in a cubic box of  $500h^{-1}\text{Mpc}$  on a side. It assumes a  $\Lambda\text{CDM}$  cosmology with parameters  $\Omega_m = 0.25$ ,  $\Omega_b = 0.045$ ,  $h = 0.73$ ,  $\Omega_\Lambda = 0.75$ ,  $n = 1$ , and  $\sigma_8 = 0.9$ , where the Hubble parameter is  $H_0 = 100 h^{-1}\text{km s}^{-1}\text{Mpc}^{-1}$ . The simulation follows 2160<sup>3</sup> dark matter particles of mass  $8.6 \times 10^8 h^{-1}M_\odot$ . Since dark matter haloes are required to contain at least 20 particles, the minimum halo mass is  $1.7 \times 10^{10} h^{-1}M_\odot$ , with a corresponding baryonic mass of about  $3.1 \times 10^9 h^{-1}M_\odot$ .

The galaxy formation model itself follows the evolution of baryons from when they collapse into a hot gas phase, through cooling onto a disk where stars can form. As the most massive stars die, supernovae (SN) eject energy into the surrounding medium, reheating the cold gas back into the hot phase or even ejecting it into the external reservoir. The black hole evolution is modeled and in massive galaxies the mechanical heating from its quiescent growth suppresses the cooling. Mergers generate star formation bursts and, depending on the mass ratio between the galaxies, disks are destroyed to form bulges. Finally dust and stellar popula-

tion synthesis models transform the predicted quantities into galaxy properties that can be compared with observations.

With all the recipes in place, the model is able to predict reasonably well the shape of the luminosity function in different bands, the stellar mass function, the galaxy colours, the black hole-bulge mass relation, the metallicity of stars, the Tully-Fisher relation, etc. However some challenges remain. For example, as happens with most current SA recipes, this model has known problems in correctly predicting the properties of dwarf galaxies (Croton et al. 2006; Weinmann et al. 2006; Henriques et al. 2008, 2009) and it has no predictions for the intra-cluster light, a component that can be substantial for the largest groups in the local Universe.

These two aspects lead us to introduce a new physical recipe: the stripping of stellar material from satellite galaxies due to the tidal forces they experience from the central companions. By removing this material from merging galaxies we expect to decrease their size and hence the number density of low-mass galaxies (where an excess is seen in the original model). At the same time, by moving the disrupted material into the intra-cluster medium (ICM) we will be able to predict the properties of the ICL. Moreover, since this corresponds to stars that would otherwise end up in the central galaxies of large groups and clusters, we expect to see considerable changes in the properties of the most massive objects in the model.

To introduce the new physics we use the implementation proposed by Taylor & Babul (2001) and follow the radial position of satellites as they merge into central objects. At each location, we compute the radius relative to the satellite centre at which the sum of the tidal force from the parent halo and the centrifugal force equal the self-gravitational force of the satellite. Any material outside this radius at each time step is considered to be unbound and is moved from the satellite galaxy into the ICM.

We assume that disruption of stellar material only acts on galaxies that have experienced large enough tidal forces to completely strip their dark matter component (for those who are aware of the Munich SA terminology, type 2 galaxies).

## 2.1 Dynamical Friction

The original model of DLB07 follows the merging of satellites by simply setting up a “merging clock”, whenever a satellite loses its dark matter halo. After this time is elapsed the galaxy is assumed to merge with its central companion.

The merging time is calculated using the Chandrasekhar (1943) formula for the dynamical friction force acting on the satellite, as described in Binney & Tremaine (1987):

$$F_{\text{df}} = -\frac{4\pi G^2 m_{\text{sat}}^2 \ln(\Lambda) \rho B(x)}{v_{\text{sat}}^2}, \quad (1)$$

where  $m_{\text{sat}}$  represents the satellite mass,  $\ln(\Lambda)$  is the Coulomb logarithm (assumed to be  $\ln(1 + m_{\text{halo}}/m_{\text{sat}})$ ),  $\rho$  is the local density and  $v_{\text{sat}}$  represents the orbital velocity of the satellite within the halo.  $B(x)$  is the error function and we take  $x = |v_{\text{sat}}|/\sqrt{2}\sigma_{\text{halo}} = 1$ , where  $\sigma_{\text{halo}}$  represents the 1-D velocity dispersion of the halo.

Assuming circular orbits and an isothermal distribution

of the total mass in haloes, the previous equation can be integrated to give the merging time:

$$t_{\text{df}} \approx 1.17 \frac{V_{\text{vir}} r_{\text{sat}}^2}{G m_{\text{sat}} \ln(\Lambda)}, \quad (2)$$

where  $r_{\text{sat}}$  is the halocentric radius of the satellite at the time that it lost its dark matter halo and  $V_{\text{vir}}$  is the virial velocity of the central halo.

For our implementation we use the same equation, but we now record the orbital radius of the satellite as it falls towards the halo centre. In this way, at each time step, we can compute the forces acting on the satellite at that radius and determine the amount of stellar material that becomes unbound.

We note that the drag force acting on satellites and causing them to merge with central objects depends on their mass. Because of this, despite us using the same equation for the dynamical friction as in DLB07, the implementation of satellite mass loss will change the predicted merging times. As satellites lose their stellar material the drag force they experience will decrease, causing them to survive longer before being accreted by the central galaxy.

## 2.2 Tidal Disruption

The mass loss on satellites occurs through the action of tidal forces. Assuming a slowly-varying system (a satellite in a circular orbit) with a spherically-symmetric mass distribution, material outside the tidal radius will be stripped from the satellite. This radius can be identified as the distance from the satellite centre at which the radial forces acting on it cancel out (King 1962; Binney & Tremaine 1987). These forces are the gravitational binding force of the satellite, the tidal force from the central halo and the centrifugal force. Using the King (1962) model and as described in Taylor & Babul (2001) the disruption radius  $r_t$  will be given by:

$$r_t \approx \left( \frac{G m_{\text{sat}}}{\omega_{\text{sat}}^2 - d^2\phi/dr^2} \right)^{1/3}, \quad (3)$$

where  $\omega_{\text{sat}}$  is the orbital angular velocity of the satellite and  $\phi$  represents the potential of the halo.

Using the isothermal sphere approximation for the mass distribution of the central halo and satellite galaxy, and assuming that the satellite follows a circular orbit, equation 3 can be rewritten as:

$$r_t \approx \frac{1}{\sqrt{2}} \frac{\sigma_{\text{sat}}}{\sigma_{\text{halo}}} r_{\text{sat}}, \quad (4)$$

where  $\sigma_{\text{sat}}$  and  $\sigma_{\text{halo}}$  are the velocity dispersions of the satellite and the halo, respectively, the former being estimated just before it becomes stripped.

The material outside this radius is assumed to be disrupted and becomes part of the ICM. We assume that the galaxy as a uniform metallicity distribution so that equal fractions of stellar mass and metals are stripped away from the galaxy. We keep following the satellites until their orbital radius becomes smaller than the sum of the radii of the central and satellite galaxies, at which point we assume a merger has occurred.

To compute the forces acting on satellite galaxies, we assume that the total mass follows a spherically-symmetric

isothermal sphere. However, to determine the amount of material outside the disruption radius that is lost at each time step, we use appropriate distribution models for the stellar mass in the different galaxy components. The model naturally defines galaxies as a combination of a disc and a spheroid. We now explain how these two components are modelled.

### 2.2.1 Mass Distribution in Disks

We model the disc component as an exponential mass distribution given by:

$$M_{\text{disk}}(< R) = \int_0^R 2\pi R \Sigma_{d,0} \exp^{-R/R_d} dR, \quad (5)$$

where  $\Sigma_{d,0}$  gives the surface density of the disk and the disk scale-length ( $R_d$ ) is calculated using the formalism derived by Mo et al. (1998). Integrating equation 5, the disk mass inside a given radius  $R$  is given by:

$$M_{\text{disk}}(< R) = M_{\text{disk}} \left[ 1 - \left( 1 + \frac{R}{R_d} \right) \exp^{-R/R_d} \right]. \quad (6)$$

### 2.2.2 Mass Distribution in Bulges

The mass in bulges is spherically symmetric distributed according to an  $r^{1/4}$  law:

$$\Sigma_{\text{bulge}} = \Sigma_{b,0} \exp^{-7.67 \left[ \left( \frac{R}{R_b} \right)^{1/4} - 1 \right]}, \quad (7)$$

where  $\Sigma_{b,0}$  gives the surface density of the bulge at the effective radius,  $R_b$ , that contains half the projected light. However, the integral to turn this into mass as a function of radius has no analytic solution and so we use the following approximation instead:

$$M_{\text{bulge}}(< r) = M_{\text{bulge}} \int_0^{r/a} \frac{x^2}{x(1+x)^3} dx, \quad (8)$$

where  $M_{\text{bulge}}$  is the total stellar mass of the bulge and the auxiliary variable  $x = R/a$  where  $a = 0.56R_b$ . Integrating equation 8, the bulge mass inside a given radius  $r$  is given by

$$M_{\text{bulge}}(< r) = M_{\text{bulge}} \frac{r^2}{r^2 + a^2}. \quad (9)$$

The pioneering work of Kormendy (1977) demonstrated that there is a correlation between the effective radius ( $R_b$ ) and the effective surface brightness ( $I$ ) of ellipticals galaxies. At the same time, Faber & Jackson (1976) showed that the luminosity of these galaxies is proportional to the velocity dispersion, with the derived relation  $L \propto \sigma^4$  expressing the intuitive notion that more luminous galaxies have higher velocity dispersions (and hence higher masses). From these two correlations, and since  $L = \pi R_b^2 I$ , it follows that the effective radius  $R_b$  should be correlated with the velocity dispersion  $\sigma$ . Since the velocity dispersion is an intrinsic quantity of theoretical galaxies derived from the properties of their host halos, we can use it to determine the effective radius and the mass distribution of bulges. To do so, we use the proportionality law from Djorgovski & Davis (1987):

$$\log(\sigma/\text{km s}^{-1}) = 0.21 \log(R_b/h^{-1} \text{pc}) + 2.58. \quad (10)$$

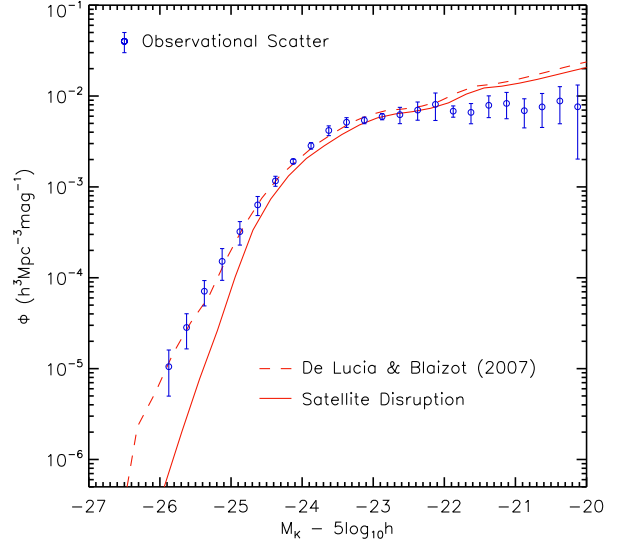


**Figure 1.** Comparison of the predicted  $K$ -band luminosity function at  $z = 0$ , from DLB07 (dashed red line) and the satellite disruption model (solid red line). The data points represent the mean of a combined set of observations from (Cole et al. 2001; Bell et al. 2003; Jones et al. 2006), with error bars reflecting the minimum and maximum estimates from the three data sets in each bin.

## 3 PREDICTIONS FROM THE DLB07 MODEL WITH GALAXY DISRUPTION

In order to better understand the changes introduced by the new physics, we start by plotting the new model predictions leaving the parameters governing the other physics unchanged from the values in DLB07. In the next section we will use the techniques introduced in Paper 1 to find a new best fit, tuning the parameters governing the basic physics of the model in order to agree with a range of observations.

### 3.1 The Luminosity Function

In Fig. 1 we plot the  $K$ -band luminosity function for the new model with satellite disruption. The predictions at redshift zero are compared with the values from the original DLB07 model and with a combination of three different observational data sets (Cole et al. 2001; Bell et al. 2003; Jones et al. 2006), respectively from 2DFGRS, 2MASS and 6DFGRS. The final data points are given by the average of the maximum and minimum number density estimates in each magnitude bin, with errors  $\sigma_i$  equal to half the difference between them. The scatter in the combined observational luminosity function represents the level of accuracy that we require from the model.

The introduction of satellite disruption into the model has a considerable effect on the bright end side of the  $K$ -band luminosity function. In the framework of a hierarchically growing Universe, these objects grow from material received during numerous mergers over their lifetime. With the inclusion of satellite disruption, a large amount of material which would otherwise end up in the brightest objects at redshift zero is transferred from satellites into the ICM. The result is an excessively low number density of bright

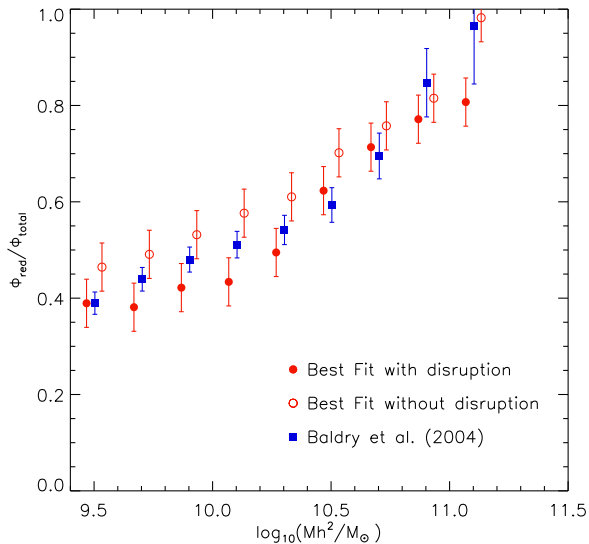


**Figure 2.** The predicted fraction of red galaxies as a function of stellar mass. The original De Lucia & Blaizot (2007) model (open red circles) is compared with the satellite disruption model (filled red circles) and observational data from Baldry et al. (2004) (filled blue squares).

objects in the  $K$ -band when compared to observations and the previous model.

The number density of dwarf galaxies is, in its turn, less affected than we inferred in Henriques et al. (2008). With the self-consistent implementation, disruption is no longer an instantaneous and dramatic process; instead galaxies lose material slowly as they follow their route into the central galaxy. Moreover, the merger time-scale is increased because satellites become smaller and less affected by dynamical friction as they spiral inwards. Nevertheless, the decrease in the number density of dwarfs is still statistically significant, due to the large numbers of these objects contained in the Universe.

We emphasize that the poor fit results from the fact that we used parameters values tuned for the basic physics, without the inclusion of satellite disruption. This makes it easier to understand the changes introduced by the new recipe. In the next section, we will test if there is a region in parameter space where disruption can produce an overall better agreement between the predicted and observed luminosity functions.

### 3.2 Galaxy Colours

In Fig. 2 we show the fraction of red galaxies as a function of stellar mass. We divide the galaxies into the two populations using the selection criteria in Weinmann et al. (2006),  $(g-r) = 0.7 - 0.032(M_r - 5 \log h + 16.5)$ , converted into a cut on the colour-stellar mass relation at redshift zero,  $(B-V) = 0.065 \log(M_* h^2/M_\odot) + 0.09$ . The conversion from the  $g-r$  to the  $B-V$  colour was done following Fukugita et al. (1996),  $g-r = 1.05(B-V) - 0.23$ . The fraction of red galaxies for different mass bins is then compared with observations from Baldry et al. (2004). The observational masses based on the ‘diet’ Salpeter IMF (Bell et al.

2003) were reduced by 0.15 dex to agree with the IMF assumed in our SA model (Chabrier 2003). The predictions from the model with satellite disruption are compared with the DLB07 model (open red circles) and observational data from Baldry et al. (2004) (filled blue squares). The disruption of stellar material from satellites significantly reduces the fraction of red galaxies over all mass ranges.

This reduction comes about through the removal of predominantly red stars from galaxies into the ICM. For central, mostly high-mass galaxies in halos, this reduces the mass of material accreted from merging dwarfs.

### 3.3 The Black Hole-Bulge Mass Relation

In Fig. 3 we show the black hole-bulge mass relation for the satellite disruption model. The colours follow the number density of objects with blue representing low and green high density regions. In comparison with the predictions for the original model (Fig. 5 in Paper 1), there is an overall reduction in the masses of both bulges and of black holes.

The reduction on black hole masses is determined by the black hole growth implementation in the model. The build up in black hole mass in the original DLB07 model is mostly due to the quasar mode:

$$\Delta m_{\text{BH,Q}} = \frac{f_{\text{BH}}(m_{\text{sat}}/m_{\text{central}}) m_{\text{cold}}}{1 + (280 \text{ km s}^{-1}/V_{\text{vir}})^2}. \quad (11)$$

This equation represents the fact that, during a merger event, the amount of cold gas driven into the central black hole depends on the instabilities created. The instabilities themselves depend on the mass ratio between the two merging galaxies. Satellite disruption decreases the overall mass of satellites, reducing the instabilities created during mergers and hence the black hole growth due to cold gas accretion.

Looking at Fig. 3 we see that the reduction in black hole growth is more significant than in bulge growth. The peak previously seen around a bulge mass of  $10^{10} M_\odot$  and a black hole mass of  $10^8 M_\odot$  has been reduced, with objects moving to lower black hole masses.

### 3.4 Intra-Cluster Light

One of the greatest advantages of introducing stellar disruption into semi-analytic models is that it naturally explains the production of intra-cluster material. For the original set of parameters the disruption model predicts ICL fractions of approximately 22 per cent for the most massive clusters of galaxies  $M_{\text{vir}} = 10^{15} M_\odot$ . In section 5.7 we will compare these predictions with those of an optimized model for virial masses ranging from  $10^{12}$  to  $10^{15} M_\odot$ .

### 3.5 The Metallicity of Stars

Apart from the galaxy quantities that originally motivated the introduction of a new recipe into the SA model, there is another predicted property that is significantly improved by the disruption of satellite galaxies. In Fig. 4 we show the metallicity of stars as a function of the galaxy stellar mass. The new disruption model (solid red lines) is compared with the original DLB07 predictions (dashed red lines) and with

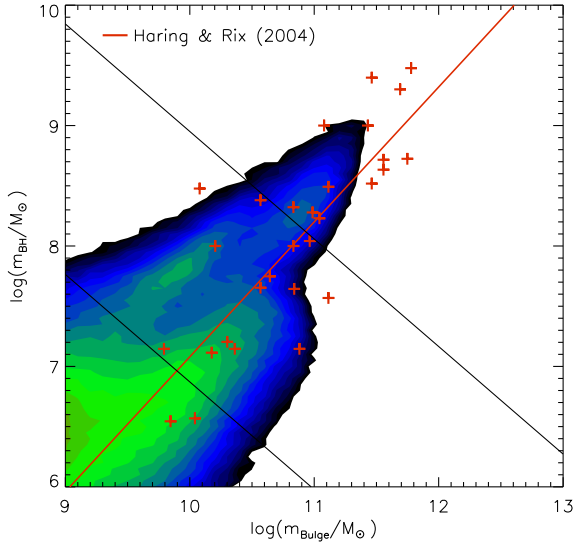


**Figure 3.** The black hole-bulge mass relation for the satellite disruption model (solid contours). The red crosses represent observations from Häring & Rix (2004) with the best fit to the data points given by the red line. The black lines represent the binning used to compare the model with observations in sections 4 and 5.

observations from Galazzi et al. (2005) (blue squares and lines). The central line represents the median value of metallicity in each mass bin (the blue squares for the observational data), while the upper and lower lines represent the 16th and 86th percentiles of the distribution. From the figure it is clear that satellite disruption improves the agreement between SA predictions and observations, by increasing the metallicity of intermediate and high mass galaxies,  $M_* > 10^{10} M_\odot$ . The explanation for this effect is related to the decrease of the number density of the most massive galaxies. With the implementation of disruption, a considerable amount of material that would otherwise end up in these objects is now transferred into the ICL. In terms of the metallicity of stars, this results in massive objects receiving less low metallicity material from satellites, hence increasing their mean metallicity.

#### 4 MCMC PARAMETER ESTIMATION

In Paper 1 we have implemented MCMC sampling in the Munich SA model. This technique allows us to combine the constraining power from multiple observational data sets with a fast sampling of high-dimensional parameter spaces. By doing so we can verify the level of agreement with observations and the relative weight of different observations in the final choice of the parameters in the best fit model, in a statistically-consistent way. Moreover, whenever reasonable agreement proves to be impossible, it helps us understanding whether there is a failure in determining the right parameter configuration, whether there is a fundamental problem with the underlying model, or whether the introduction of new physics is required.

In the previous section we presented the predictions for the SA model with a self-consistent treatment of the dis-

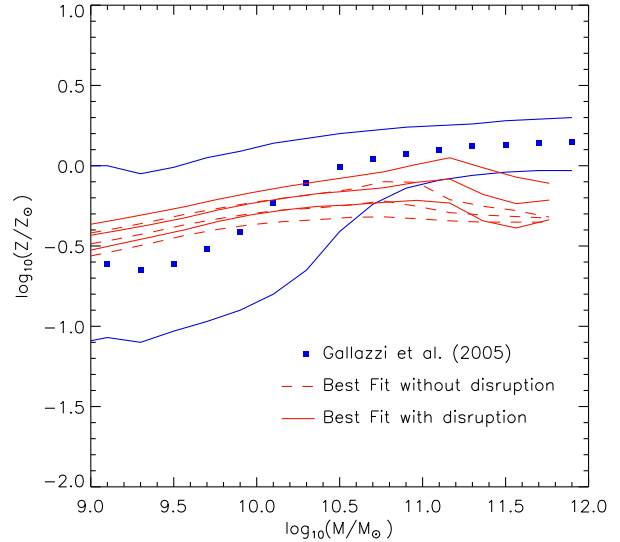


**Figure 4.** Comparison between the metallicity of stars in the satellite disruption model (solid red lines), in De Lucia & Blaizot (2007) (dashed red lines) and in observations from Galazzi et al. (2005) (blue squares and lines). For all the data sets, the central line represents the median value of metallicity in each mass bin (the blue squares for the observational data), while the upper and lower lines represent the 16th and 86th percentiles of the distribution.

ruption of satellite galaxies. These were obtained using the parameters from the original model of DLB07, not adjusted to incorporate this new physical recipe. In this section, we will use the MCMC sampling techniques introduced in Paper 1 to search for the combination of parameters that gives the best fit for the satellite disruption model. We refer the reader to that paper for a full description of the statistical methods. The same MCMC implementation is used, namely the Metropolis-Hastings algorithm (Metropolis et al. 1953; Hastings 1970) and a log-normal proposal distribution with a width that assures an overall acceptance rate in each chain between 10% and 40%.

Due to the computational requirements, we will once more perform the sampling in a single volume of the millennium simulation, representing 1/512 of the total simulation. Since we choose a representative file, with a luminosity function and mean density similar to that of the total volume, we are able to correctly constrain the properties of galaxies in all mass ranges except for the most massive objects ( $M_* > 10^{11} M_\odot$ ). The MCMC sampling is performed over  $\sim 30\,000$  steps and the output analyzed using GETDIST, which is part of the COSMOMC software package (Lewis & Bridle 2002), adapted to produce 1d and 2d maximum likelihood (profile) and MCMC marginalised (posterior) distributions. Once the best fit parameters are obtained, we then re-run the SA code over the entire Millennium to obtain the galaxies properties presented later in this paper.

Using one file representative of the total volume significantly reduces the computational time required for our study. Nevertheless, the size of the calculations involved, even in that smaller volume, still make it a challenging task.

**Table 1.** SA model parameters from De Lucia & Blaizot (2007). The first 6 parameters are frozen in our analysis at the values shown here.

$f_b$	$z_0$	$z_r$	$T_{\text{merger}}$	$R$	$Y$
0.17	8	7	0.3	0.43	0.03
$\alpha_{\text{SF}}$	$k_{\text{AGN}}$	$f_{\text{BH}}$	$\epsilon_{\text{disk}}$	$\epsilon_{\text{halo}}$	$\gamma_{\text{ej}}$
0.03	$7.5 \times 10^{-6}$	0.03	3.5	0.35	0.5

In order to perform the sampling, the Cosmology Machine (COSMA) supercomputer supplied by Sun Microsystems was used, a machine based in the Durham University that is part of the Virgo Consortium facilities.

#### 4.1 Model Parameters

As in Paper 1, in order to better understand the basic physics of the model, we choose to do our MCMC sampling only on 6 of 12 parameters in the model. On the top line of table 1 we show the frozen parameters corresponding to the baryon fraction ( $f_b$ ), the redshifts of beginning and end of reionization (respectively  $z_0$  and  $z_r$ ), the major to minor merger threshold ( $T_{\text{merger}}$ ), the instantaneous recycled fraction ( $R$ ) and the yield of metals ( $Y$ ). On the bottom line, we show the values for the more fundamental parameters that we choose to sample. These are the star formation efficiency ( $\alpha_{\text{SF}}$ ), the AGN radio mode efficiency ( $k_{\text{AGN}}$ ), the black hole growth efficiency ( $f_{\text{BH}}$ ), the SN reheating and ejection efficiency (respectively  $\epsilon_{\text{disk}}$  and  $\epsilon_{\text{halo}}$ ) and ejected gas reincorporation efficiency ( $\gamma_{\text{ej}}$ ). The physics governed by all the parameters are fully described in Croton et al. (2006) as well as in Paper 1.

#### 4.2 Observational Constraints

The comparison between model and observations will be done using the same data sets and statistical tests as before and since we have not introduced any additional parameter, the relative goodness of the original and the satellite disruption model can be assessed directly. The ability or not for the MCMC to find a best fit model with a likelihood higher than before will tell us if the introduction of the new physical recipe is justified.

The three observations used are the  $K$ -band luminosity function, the fraction of red galaxies versus stellar mass and the black hole-bulge mass relation. For a detailed description of the observational data sets and the statistical tests employed, we refer the reader to Paper 1.

## 5 RESULTS FROM THE OPTIMISED STRIPPING MODEL

### 5.1 The Best Fit Semi-Analytic Model with Satellite Disruption

We now present the results for the MCMC sampling when the SA model with satellite disruption is constrained by the three observational data sets combined. The likelihood for

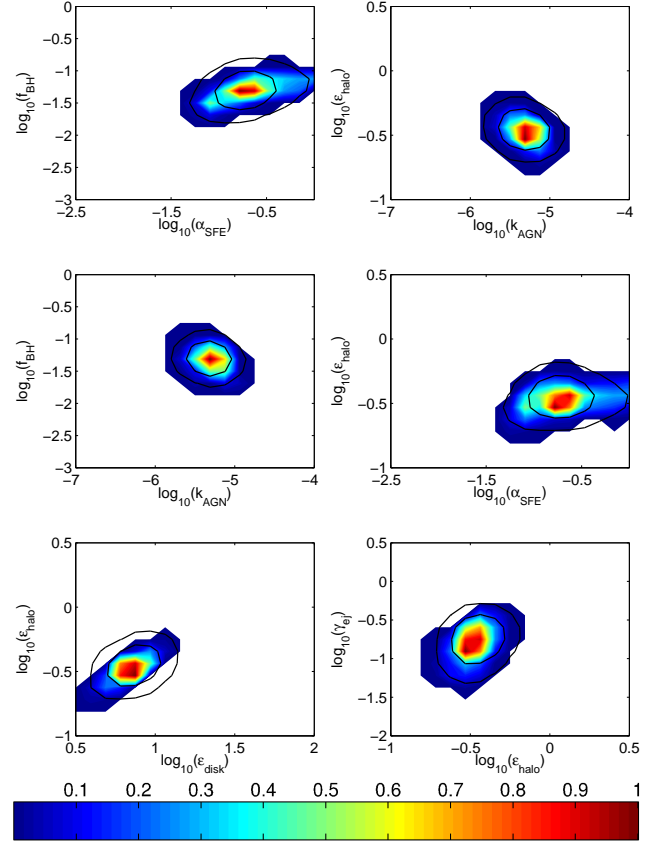


**Figure 5.** Correlations between the 6 parameters analysed in the study for the SA model with satellite disruption constrained by three observational properties: the  $K$ -band luminosity function, the fraction of red galaxies, and the black hole-bulge mass relation. The values of the parameters are plotted in log space, with the solid contours representing the 68% and 95% preferred regions from the MCMC (the posterior distribution) and the colours the maximum likelihood value sampled in each bin (the profile distribution). The colour scale is normalized by the maximum likelihood value of 0.15.

the best fit model is given by the product of the likelihood from the three statistical tests:

$$\pi(x_i) = \mathcal{L}_{(K\text{-band})} \times \mathcal{L}_{(\text{Colour})} \times \mathcal{L}_{(\text{BH-Bulge})}. \quad (12)$$

Fig. 5 shows the allowed ranges and correlations between the parameters sampled. As in Paper 1, the use of combined observations to produce one comprehensive data set in terms of galaxy formation properties restricts the parameters to one small region with acceptable likelihood.

The original model had a maximum likelihood value of just 0.037 when compared with the chosen set of observational constraints, meaning it was formally ruled out at a  $2\text{-}\sigma$  level. However, the new satellite disruption recipe brings the model likelihood up to 0.15. Since we introduced no additional parameters, this increase in a factor of 4 in peak likelihood means that the inclusion of the new physical process seems to be favoured by data.

In comparison to our analysis for the model without galaxy disruption, we see both an increase in the likelihood value of our best fit and in the allowed regions in parameters space. This is mainly caused by the changes that the new physical recipe produces on the black hole-bulge mass

relation. The regions required in parameter space by the different tests now have a much larger overlap. This means that the black hole and bulge mass build up in the new model is now consistent with the other galaxy properties analyzed, namely the  $K$ -band luminosity function and the fraction of red galaxies.

In order to understand the changes introduced by satellite disruption we include two additional plots in our analysis (the two top panels in Fig. 5), the correlations between the AGN quasar mode parameter and the star formation efficiency, and the AGN radio mode and the disk reheating efficiency.

An expected correlation, but one that was not seen in Paper 1 is shown in the upper left panel. A positive correlation is now evident between the quasar mode, responsible for the black hole growth, and the star formation efficiency, responsible for the bulge growth. Considering the physics governed by them, it comes at no surprise that an increase in one requires an increase in the other in order to maintain the black hole-bulge mass fraction of galaxies. The fact that this correlation was not present in the previous study is explained by the considerably smaller regions with acceptable likelihood that we found before.

For the same reason, the correlation between the supernova reheating and ejection parameters, produced by the  $K$ -band luminosity constraint, is now clear in the lower left corner. As explained in Paper 1 this correlation keeps the virial velocity cutoff, above which SN feedback stops being effective, at a constant value:

$$V_{\text{vir},0} = \left( \frac{\epsilon_{\text{halo}}}{\epsilon_{\text{disk}}} \right)^{\frac{1}{2}} V_{\text{SN}}. \quad (13)$$

This means that this form of energy only suppresses star formation in the smallest objects where an excess compared to observations was previously seen.

Accordingly, the lower and middle right panels show an identical behaviour for the parameters as in the  $K$ -band sampling on Paper 1. An increase in the amount of gas ejected by SN needs to be balanced by an increase in the reincorporation time-scale and the star formation efficiency.

## 5.2 Best Fit Parameters and Confidence Limits

The best fit and confidence limits for the 6 free parameters in the model with satellite disruption, together with the published values from DLB07 and the best fit for the model without satellite disruption are shown in table 2. Despite a different model being used, the parameters from both the original DLB07 and the previous MCMC analysis remain close to the new  $2\sigma$  confidence limits.

In comparison to the best fit obtained for the model without satellite disruption, the most dramatic effect in terms of preferred parameter values is the increase in the star formation efficiency. It represents a change in the fraction of cold gas transformed into stars in a disk dynamical time from 4% to 16%. Such an increase is required to repopulate the bright end side of the  $K$ -band luminosity function, largely affected by disruption. This effect is somewhat balanced by an increase in the mechanical heating from AGN, given by the product of  $k_{\text{AGN}}$  and  $f_{\text{BH}}$ .

The virial velocity cutoff, above which supernova stops being effective (Eq. 13), is similar to that found for the model

without disruption. This means that the new model still requires the supernova feedback to be effective only for small objects. However, the strength required from this form of feedback is now smaller (6.94 for the reheating and 0.33 for the ejection efficiency), which seems to be in better agreement with observations (Martin 1999). This means that disruption does indeed help reducing the excess of dwarfs in the model and that an excessively strong feedback is no longer required.

## 5.3 Predictions for the Best Fit Satellite Disruption Model

In this section we analyze the predictions from the best fit model with satellite disruption. Contrary to the MCMC sampling, done in a single volume due to computational resource limitations, the following predictions were obtained using the full Millennium Simulation.

## 5.4 Galaxy Luminosity Functions

In the left panel of Fig. 6 the  $K$ -band luminosity functions from the best fit for DLB07 and the best fit for the satellite disruption models are plotted against the observational data set used to constrain the sampling. In comparison to the best fit obtained for a model without disruption the new model produces similar galaxy luminosities. However, for the model including satellite disruption, the good agreement at the low luminosity end is achieved with a less efficient supernova feedback, which seems to be in better agreement with observations.

In the right panel of Fig. 6 we show the predictions for the  $b_J$ -band luminosity function. The best fit satellite disruption model is compared with the best fit for DLB07 and two observational data sets. As for the  $K$ -band, both best fit models with and without disruption show produce similar predictions, achieving an overall good agreement with observations, except for the region around  $L_*$ . We note however that the  $b_J$ -band flux is highly dependent on the adopted dust model (which does not happen with the other properties analyzed). For this reason, the excess just mentioned can be removed by adjusting the dust implementation, without affecting the agreement achieved for the other galaxy properties. We choose not to do so, in order to make more clear the changes introduced by satellite disruption.

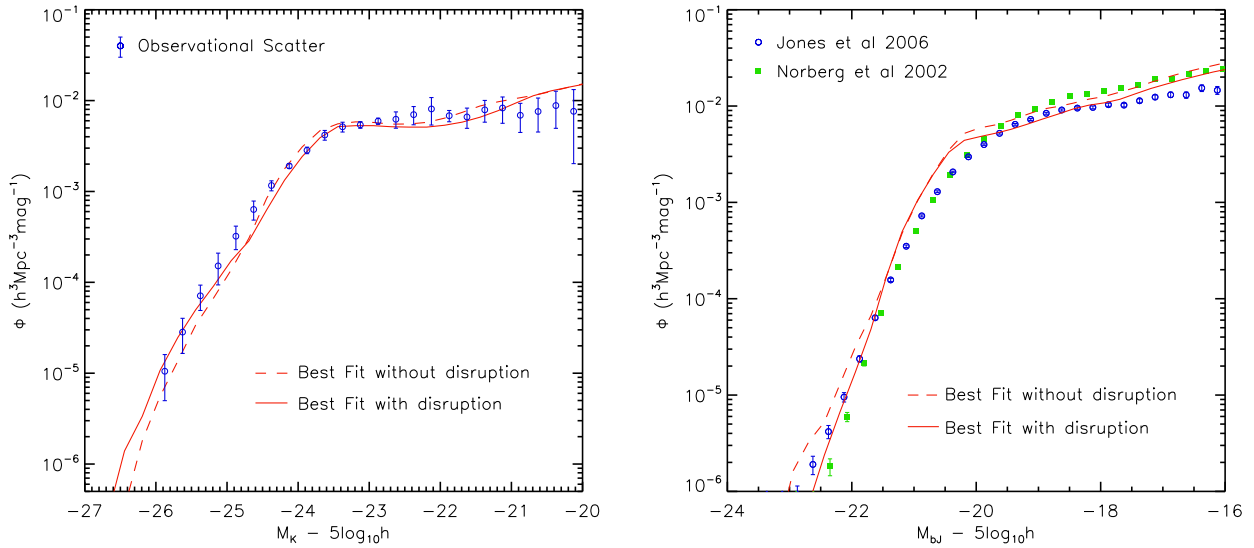
## 5.5 Galaxy Colours

Fig. 7 shows the predictions for the galaxy colours in the best fit model with satellite disruption. The top panel gives the  $B-V$  colour-stellar mass relation (colour coded by the number density of objects), while the bottom panel shows the fraction of red over the total number of galaxies as a function of stellar mass. The introduction of disruption without changing the original DLB07 parameter values decreases the overall fraction of red galaxies, causing the model to under-predict the number of these objects except for  $L_*$  galaxies (Fig. 2). As seen in the bottom panel of Fig. 7, the MCMC optimization brings the model into agreement with observations for the entire plotted range. When compared to the best fit without disruption, the new model produces



**Table 2.** Statistics from the MCMC parameter estimation for the parameters in the satellite disruption model. The best fit and marginalized confidence limits are compared with the published values from De Lucia & Blaizot (2007) and with the best fit values obtained without the inclusion of satellite disruption (Paper 1).

	DLB07	Paper 1	Disruption Model	$-2\sigma$	$-1\sigma$	$+1\sigma$	$+2\sigma$
$\alpha_{SF}$	0.03	0.039	0.17	0.078	0.13	0.28	0.53
$k_{AGN}$	$7.5 \times 10^{-6}$	$5.0 \times 10^{-6}$	$5.3 \times 10^{-6}$	$2.7 \times 10^{-6}$	$3.7 \times 10^{-6}$	$6.2 \times 10^{-6}$	$7.9 \times 10^{-6}$
$f_{BH}$	0.03	0.032	0.047	0.030	0.041	0.061	0.075
$\epsilon_{disk}$	3.5	10.28	6.86	5.22	6.33	8.51	10.11
$\epsilon_{halo}$	0.35	0.53	0.33	0.26	0.31	0.40	0.46
$\gamma_{ej}$	0.5	0.42	0.13	0.076	0.12	0.24	0.30



**Figure 6.** Comparison of the predicted  $K$ -band (left panel) and  $b_J$ -band (right panel) luminosity functions at  $z = 0$  from the best fit for DLB07 (dashed red line) and the best fit for the satellite disruption model (solid red line). On the left panel, the data points represent the observations used to constrain the luminosities of galaxies in the MCMC parameter estimation (Cole et al. 2001; Bell et al. 2003; Jones et al. 2006). On the right panel, the  $b_J$ -band luminosity function is compared with observations from 2DFGRS (green filled squares) and 6DFGS (blue open circles), respectively Norberg et al. (2002) and Jones et al. (2006).

an overall better agreement with observations, reducing the systematic excess of small galaxies previously seen (open red circles).

More interesting is that the model now starts to produce an isolated population of massive red galaxies, as required by observations (top panel of Fig. 7). However, despite reducing the number of dwarf red galaxies, the disruption model still has an excessive fraction of these objects when compared to observations.

## 5.6 The Black Hole-Bulge Mass Relation

The changes introduced by satellite disruption in the predicted black-hole bulge mass relation are the main reason for the better fit obtained in the new model. This means that the allowed likelihood region for the  $K$ -band luminosity function and for the fraction of red galaxies now produces black hole and bulge masses that agree with observational results.

As explained in section 3.3, disruption has a large im-

pact on both black hole and bulge masses. However, looking at the distribution of these masses in the best fit model, it becomes clear that the higher likelihood obtained is largely due to the reduction in black hole growth. The small sizes of the satellites will mean that smaller instabilities are created during mergers and that smaller amounts of cold gas are driven into the central black holes.

In Fig. 8 we show the black hole-bulge mass relation for the satellite disruption model with the best fit parameters. The peak around bulge masses of  $10^{10} M_{\odot}$  and black hole masses of  $10^8 M_{\odot}$  has disappeared. This means that most of the intermediate mass bulges and black holes are now on or below the observational red line, where most observational points are located. The binomial test used produces a probability three times higher than before.

## 5.7 The Intra-Cluster Light

In Fig. 9 we plot the predicted ICL from our best fit model with satellite disruption. The solid line represents the me-

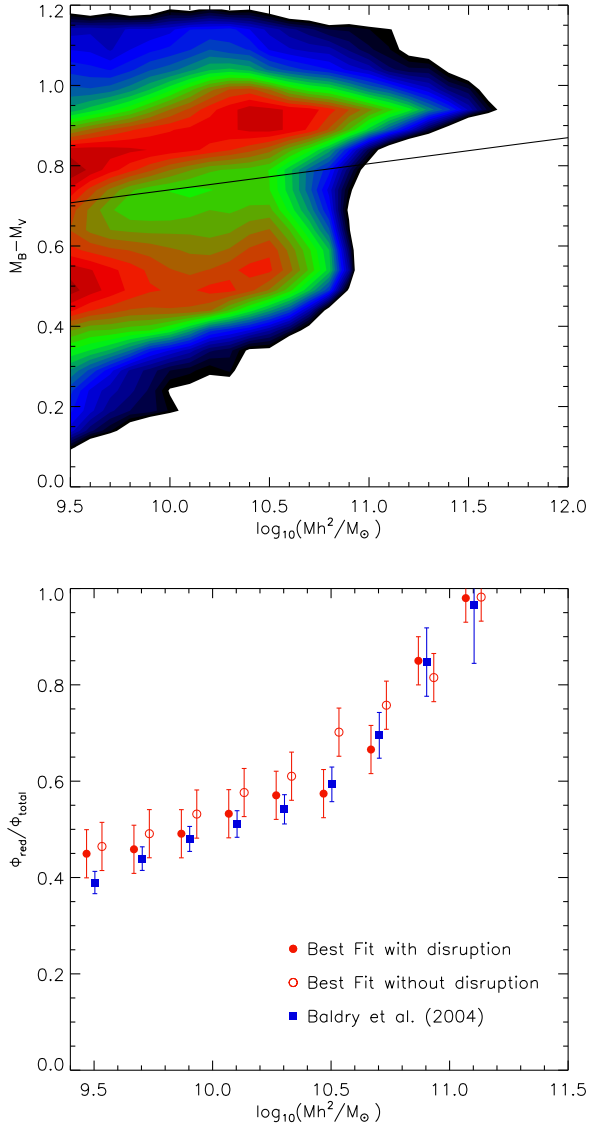


**Figure 7.** The top panel shows the  $B-V$  colour-stellar mass relation for the galaxies in the best fit satellite disruption model. The solid line represents the division between the red and blue populations in Weinmann et al. (2006). The predicted fraction of red galaxies as a function of stellar mass is shown in the bottom panel. The best fit for the original DLB07 model (open red circles) is compared with the best fit for the satellite disruption model (filled red circles) and observational data from Baldry et al. (2004) (filled blue squares).

dian of the  $M_{ICL}/M_{total}$  distribution in each bin while the dashed line gives the same relation for the disruption model with the original set of parameters.

The predicted ICL fraction for groups with  $M_{vir} > 10^{13} M_{\odot}$  has a mean of  $\approx 18\%$ . This value is compatible with observations that detect ICL fractions between 10% and 40% (Bernstein et al. 1995; Gonzalez et al. 2000; Feldmeier et al. 2002, 2004; Gonzalez et al. 2005; Zibetti et al. 2005). The prediction decreases systematically as we move to smaller virial masses reaching a mean of  $\approx 7\%$  for  $M_{vir} = 10^{12} M_{\odot}$ . The difficulty in distinguishing between ICL and that from

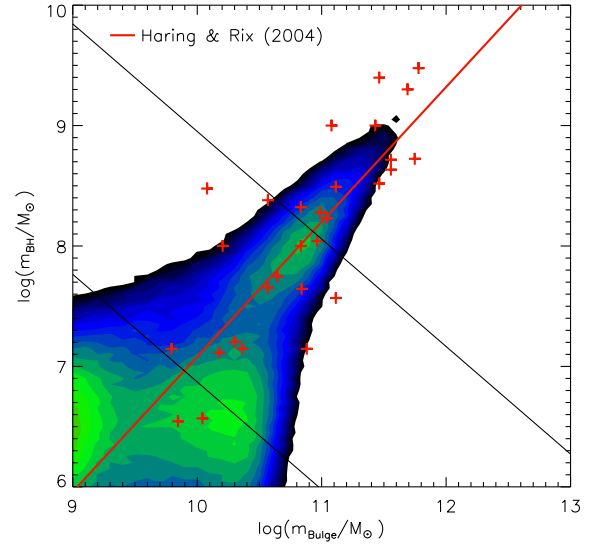


**Figure 8.** The black hole-bulge mass relation for the best fit satellite disruption model (solid contours). The red crosses represent observations from Häring & Rix (2004) with the best fit to the data points given by the red line. The black lines represent the binning used to compare the model with observations.

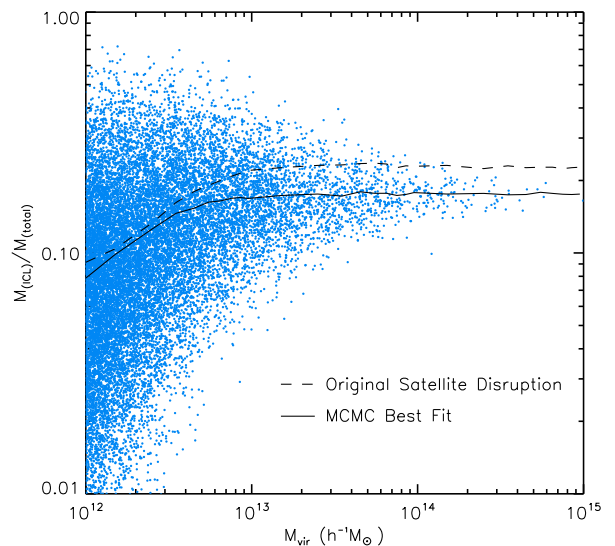


**Figure 9.** Fraction of the mass in the ICM over the total stellar mass of the group as a function of virial mass. The blue dots are a representative sample of the total galaxy population in the best fit model with satellite disruption. The solid and dashed lines represent the median of the  $M_{ICL}/M_{total}$  distribution for the satellite disruption model with the best fit and original parameters respectively.

the halo of the central galaxy (the former can be regarded as an extension of the latter), means that observational data is only available for large groups and has a considerable scatter.

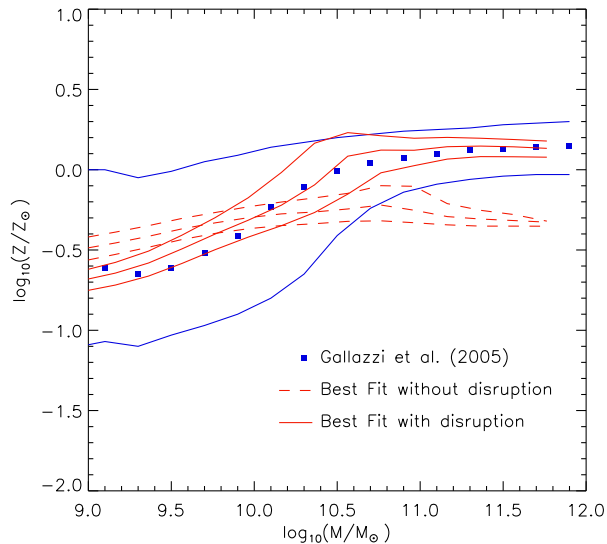


**Figure 10.** Comparison between the metallicity stars in the best fit for the satellite disruption model (solid red lines), in the best fit for DLB07 (dashed red lines) and in observations from Gallazzi et al. (2005) (blue squares and lines). For all the data sets, the central line represents the median value of metallicity in each mass bin (the blue squares for the observational data), while the upper and lower lines represent the 16th and 86th percentiles of the distribution.

## 5.8 The Metallicity of Stars

In Fig. 10 we show the metallicity of stars as a function of the galaxy stellar mass. We remind the reader that this was not one of the observations used to constrain the model. The best fit disruption model (solid red lines) is compared with the best fit for the original DLB07 (dashed red lines) and with observations from Gallazzi et al. (2005) (blue squares and lines). As in Fig. 4, the central line represents the median value of metallicity in each mass bin (the blue squares for the observational data), while the upper and lower lines represent the 16th and 86th percentiles of the distribution.

As for the best fit model without disruption, the increase in supernova feedback required by the MCMC lowers the metallicity of stars for the low mass galaxies in the best fit for the disruption model. In comparison to the original model (Fig. 4), for this mass range, the higher SN feedback from both best fit models increases the fraction of metals in the gas phase, consequentially lowering the fraction of metals in stars.

As explained in section 3.5, the introduction of disruption increases the metallicity of massive objects, by reducing the amount of low metallicity material that they receive from mergers. This means that the distribution of metals in the model is now in close agreement with observations over the entire mass range plotted.

## 6 DISCUSSION

In Paper 1, we introduced a new approach to galaxy formation modelling. Combining the MCMC sampling techniques with SA models allowed us to gain insight on the physical

importance of the different galaxy parameters. With the introduction of a new physical recipe, presented here, both the normalisation and shapes of the acceptable likelihood regions contain useful information that can be used to discriminate between models.

In this work we implement a new physical ingredient in the SA recipe: the stripping of satellite galaxies by tidal forces during merging events. The concept had already been introduced in Henriques et al. (2008), but only as an *a posteriori* study. That approach, despite enabling us to gain insight on the impact that this process would have in the population of dwarfs, did not allow us to study the effect of stripping in a self-consistent way, and in particular the effect on the most massive galaxies.

The self-consistent implementation that we describe in this chapter makes it possible to study the impact of disruption on the properties of galaxies of all types. Namely, it allows us to study the loss in mass by satellite galaxies, the slower build up of central galaxies (since they receive less material from satellites) and the growth of the ICM component, previously neglected. On top of that, the MCMC sampling allows us to learn if the new process is favoured or not by observations.

In comparison to the original model, the best fit likelihood of the model with disruption is **four times** higher with respect to the *K*-band luminosity Function, the fraction of red galaxies and the black hole-bulge mass relation.

- Since we did not introduce any additional parameter to model disruption, this means that the inclusion of tidal disruption of stellar material from satellite galaxies during mergers seems to be favoured by observations.
- Moreover, it means that the new model is now formally consistent with the combined observational data set we used.
- The higher likelihood value and the larger allowed likelihood regions in parameter space of the new best fit model are mainly determined by the changes produced by satellite disruption on the black hole-bulge mass relation. This means that the growth of bulges and black holes is now consistent with the properties of the galaxies as a whole.
- The new best fit has a considerably higher star formation efficiency in order to correct the reduction in the number density of massive objects caused by disruption. This is balanced in massive galaxies by an increase in the AGN feedback efficiency. At low masses, a less effective supernova feedback is now required, in better agreement with observations (Martin 1999).
- Although they were not used as constraints, the MCMC sampling for the new model kept the agreement with the observational *b<sub>J</sub>*-band luminosity function and significantly improved the overall shape of the metallicity distribution of stars.
- Finally, the introduction of disruption allows us to follow the build up of the ICM, which represents about 18% of the total light in clusters, in agreement with observations (between 10% and 40%).

### 6.1 Future Challenges

Despite the higher likelihood found for the best fit model, SA predictions are still far from exactly reproducing observations. From our analysis, the biggest challenge for the SA

model is still to reproduce the properties of dwarf galaxies. With the introduction of satellite disruption, the model is able to reproduce the number density of these objects with a less efficient supernova feedback, which is in better agreement with observational studies (Martin 1999).

Nevertheless, this type of galaxies remain predominantly red, in disagreement with observational studies. Stripping of stars does help reducing the number of red dwarfs, but is only part of the solution to the problem. Another important factor might be the treatment of the impact of mergers on the gas phase. For example, Font et al. (2008) consider a model in which the gas of satellite galaxies is continually, instead of instantaneously stripped, enabling them to form stars and remain on the blue sequence for longer.

The higher likelihood found for the best fit model with satellite disruption seems to be directly related to a better agreement between the black hole-bulge mass and the other two constraints. This fact is apparently related to the slower build up of black holes relative to bulges and the overall slower build up of both components. However, we emphasize the points raised in Paper 1 about the simplicity of the black hole growth model, which still appears to neglect important features such as the impact of the quasar mode feedback on galaxy properties. In addition, from an observational point of view, larger and more robust data sets of black hole properties are needed.

The predictions obtained for the ICL are in good agreement with observations. However, the available data is still subjected to large error bars, due to the difficulties in distinguish between the light from the brightest cluster galaxies and the ICM itself. Also, this component is still only detectable in large groups and clusters due to its low surface brightness. If future improvements in observations make it possible, this property could be used to directly constrain the model with satellite disruption.

## ACKNOWLEDGEMENTS

We thank all the members of the Sussex Survey Science Centre which joint expertise helped developing the innovative idea in this paper. We are grateful to Gabriella De Lucia, Guinevere Kauffmann, Volker Spingel and Simon White for providing us with the Munich SA code and for supporting our use of it.

The computations developed for this work, were performed in the Virgo Consortium cluster of computers, COSMA. The authors would like to thank Lydia Heck for its great technical knowledge about COSMA and constant feedback without which this work could not have been done.

BH acknowledges the support of his PhD scholarship from the Portuguese Science and Technology Foundation which supported him for most of the time while this work was developed. PAT was supported by an STFC rolling grant.

## REFERENCES

- Baldry I. K., Glazebrook K., Brinkmann J., Ivezić Ž., Lupton R. H., Nichol R. C., Szalay A. S., 2004, *ApJ*, 600, 681
- Bell E. F., McIntosh D. H., Katz N., Weinberg M. D., 2003, *ApJ Supp.*, 149, 289
- Benson A. J., Bower R. G., Frenk C. S., Lacey C. G., Baugh C. M., Cole S., 2003, *ApJ*, 599, 38
- Benson A. J., Frenk C. S., Lacey C. G., Baugh C. M., Cole S., 2002, *MNRAS*, 333, 177
- Benson A. J., Lacey C. G., Baugh C. M., Cole S., Frenk C. S., 2002, *MNRAS*, 333, 156
- Bernstein G. M., Nichol R. C., Tyson J. A., Ulmer M. P., Wittman D., 1995, *AJ*, 110, 1507
- Bertone S., De Lucia G., Thomas P. A., 2007, *MNRAS*
- Binney J., Tremaine S., 1987, *Galactic dynamics*. Princeton, NJ, Princeton University Press, 1987, 747 p.
- Bower R. G., Benson A. J., Malbon R., Helly J. C., Frenk C. S., Baugh C. M., Cole S., Lacey C. G., 2006, *MNRAS*, 370, 645
- Bower R. G., McCarthy I. G., Benson A. J., 2008, *MNRAS*, 390, 1399
- Bullock J. S., Kravtsov A. V., Weinberg D. H., 2001, *ApJ*, 548, 33
- Cattaneo A., Dekel A., Devriendt J., Guiderdoni B., Blaizot J., 2006, *MNRAS*, 370, 1651
- Chabrier G., 2003, *PASP*, 115, 763
- Chandrasekhar S., 1943, *ApJ*, 97, 255
- Cole S., Norberg P., Baugh C. M., et al., 2001, *MNRAS*, 326, 255
- Croton D. J., Springel V., White S. D. M., De Lucia G., Frenk C. S., Gao L., Jenkins A., Kauffmann G., Navarro J. F., Yoshida N., 2006, *MNRAS*, 365, 11
- De Lucia G., Blaizot J., 2007, *MNRAS*, 375, 2
- De Lucia G., Kauffmann G., White S. D. M., 2004, *MNRAS*, 349, 1101
- Djorgovski S., Davis M., 1987, *ApJ*, 313, 59
- Durrell P. R., Ciardullo R., Feldmeier J. J., Jacoby G. H., Sigurdsson S., 2002, *ApJ*, 570, 119
- Faber S. M., Jackson R. E., 1976, *ApJ*, 204, 668
- Faltenbacher A., Mathews W. G., 2005, *MNRAS*, 362, 498
- Feldmeier J. J., Mihos J. C., Morrison H. L., Harding P., Kaib N., Dubinski J., 2004, *ApJ*, 609, 617
- Feldmeier J. J., Mihos J. C., Morrison H. L., Rodney S. A., Harding P., 2002, *ApJ*, 575, 779
- Font A. S., Bower R. G., McCarthy I. G., Benson A. J., Frenk C. S., Helly J. C., Lacey C. G., Baugh C. M., Cole S., 2008, *MNRAS*, 389, 1619
- Fukugita M., Ichikawa T., Gunn J. E., Doi M., Shimasaku K., Schneider D. P., 1996, *AJ*, 111, 1748
- Gal-Yam A., Maoz D., Guhathakurta P., Filippenko A. V., 2003, *AJ*, 125, 1087
- Gallazzi A., Charlot S., Brinchmann J., White S. D. M., Tremonti C. A., 2005, *MNRAS*, 362, 41
- Gonzalez A. H., Zabludoff A. I., Zaritsky D., 2005, *ApJ*, 618, 195
- Gonzalez A. H., Zabludoff A. I., Zaritsky D., Dalcanton J. J., 2000, *ApJ*, 536, 561
- Granato G. L., De Zotti G., Silva L., Bressan A., Danese L., 2004, *ApJ*, 600, 580
- Gregg M. D., West M. J., 1998, *Nat.*, 396, 549
- Guo Q., White S. D. M., 2009, *MNRAS*, 396, 39
- Håring N., Rix H.-W., 2004, *ApJ*, 604, L89
- Hastings W. K., 1970, *Biometrika*, 57, 97
- Henriques B. M., Bertone S., Thomas P. A., 2008, *MNRAS*, 383, 1649

- Henriques B. M. B., Thomas P. A., Oliver S., Roseboom I., 2009, MNRAS, pp 561–+
- Jones D. H., Peterson B. A., Colless M., Saunders W., 2006, MNRAS, 369, 25
- Kampakoglou M., Trotta R., Silk J., 2008, MNRAS, 384, 1414
- King I., 1962, AJ, 67, 471
- Kormendy J., 1977, ApJ, 218, 333
- Krick J. E., Bernstein R. A., Pimbblet K. A., 2006, ApJ, 131, 168
- Lewis A., Bridle S., 2002, Phys. Rev., 66, 103511
- Martin C. L., 1999, ApJ, 513, 156
- Menci N., Fontana A., Giallongo E., Grazian A., Salimbeni S., 2006, ApJ, 647, 753
- Metropolis N., Rosenbluth A., Rosenbluth M., Teller A., Teller E., 1953, J. Chem. Phys., 21, 1087
- Mo H. J., Mao S., White S. D. M., 1998, MNRAS, 295, 319
- Monaco P., Fontanot F., Taffoni G., 2007, MNRAS, 375, 1189
- Monaco P., Murante G., Borgani S., Fontanot F., 2006, ApJ, 652, L89
- Moore B., Katz N., Lake G., Dressler A., Oemler A., 1996, Nat., 379, 613
- Murante G., Arnaboldi M., Gerhard O., Borgani S., Cheng L. M., Diaferio A., Dolag K., Moscardini L., Tormen G., Tornatore L., Tozzi P., 2004, ApJ, 607, L83
- Murante G., Giovalli M., Gerhard O., Arnaboldi M., Borgani S., Dolag K., 2007, MNRAS, 377, 2
- Napolitano N. R., Pannella M., Arnaboldi M., Gerhard O., Aguerri J. A. L., Freeman K. C., Capaccioli M., Ghigna S., Governato F., Quinn T., Stadel J., 2003, ApJ, 594, 172
- Neill J. D., Shara M. M., Oegerle W. R., 2005, ApJ, 618, 692
- Norberg P., Cole S., Baugh C. M., et al., 2002, MNRAS, 336, 907
- Rudick C. S., Mihos J. C., Frey L. H., McBride C. K., 2009, ApJ, 699, 1518
- Seek Kim H., Baugh C. M., Cole S., Frenk C. S., Benson A. J., 2009, ArXiv e-prints
- Somerville R. S., Hopkins P. F., Cox T. J., Robertson B. E., Hernquist L., 2008, MNRAS, 391, 481
- Sommer-Larsen J., Romeo A. D., Portinari L., 2005, MNRAS, 357, 478
- Springel V., White S. D. M., Jenkins A., et al., 2005, Nat., 435, 629
- Taylor J. E., Babul A., 2001, ApJ, 559, 716
- Trentham N., Mobasher B., 1998, MNRAS, 293, 53
- Weinmann S. M., van den Bosch F. C., Yang X., Mo H. J., 2006, MNRAS, 366, 2
- Weinmann S. M., van den Bosch F. C., Yang X., Mo H. J., Croton D. J., Moore B., 2006, MNRAS, 372, 1161
- Wetzel A. R., White M., 2009, ArXiv e-prints
- Willman B., Governato F., Wadsley J., Quinn T., 2004, MNRAS, 355, 159
- Yang X., Mo H. J., van den Bosch F. C., 2009, ApJ, 693, 830
- Zibetti S., White S. D. M., Schneider D. P., Brinkmann J., 2005, MNRAS, 358, 949
- Zwicky F., 1951, PASP, 63, 61